Available online at www.sciencedirect.com

SCIENCE DIRECT

Thin Solid Films 490 (2005) 137 – 141

thin solid films

www.elsevier.com/locate/tsf

Infrared study of free carriers in X/ZnO (X=semiconductor, metal) nanocomposites

J. García-Serrano[a,b], G. Casarrubias-Segura[c], A.G. Galindo[d], X. Mathew[c], U. Pal[a,*]

[a]Instituto de Física, Universidad Autónoma de Puebla, Apdo. Postal J-48, Puebla, Pue., C.P. 72570, México
[b]Centro de Investigaciones en Materiales y Metalurgia, Universidad Autónoma del Estado de Hidalgo, Carretera Pachuca Tulancingo Km 4.5, Pachuca, Hidalgo, México
[c]Centro de Investigación en Energía-UNAM, 62580, Temixco, Morelos, México
[d]Centro de Química, Instituto de Ciencias, Benemérita Universidad Autónoma de Puebla, Blvd. 14 Sur 6301, San Manuel 72570, Puebla, Pue., México

Available online 28 July 2005

Abstract

The infrared (IR) reflectance spectroscopy technique was used for the qualitative determination of free carrier density in metal and semiconductor nanocluster embedded ZnO films. The effects of incorporation of metal and semiconductor nanoclusters on the evolution of the free carrier absorption band in the nanocomposites were studied. Our results reveal that the concentration of free carriers in the composite films depends strongly on the nature of incorporated clusters in the matrix and the annealing temperature. It is demonstrated that just by monitoring the position of a single IR reflectance band, the extent of oxidation of any incorporated species in ZnO can be monitored qualitatively.
© 2005 Published by Elsevier B.V.

Keywords: Zinc oxide; Free carriers; Infrared reflectance; Nanocomposites

1. Introduction

The metal-oxide semiconductor ZnO has many technologically important applications such as transparent conductors [1], solar cell windows [2,3], gas sensors [4,5], surface acoustic wave devices [6], etc. Recent success in producing large-area single crystals has opened the possibility of using ZnO to produce UV light emitters and high-temperature, high power transistors [7,8]. While the recent progress in fabrication techniques has produced ZnO thin films and several nanostructures [9–11] with controlled morphology, the control of their electrical properties has remained difficult. Due to high resistively of ZnO in thin film form and the nature of doping materials, a direct evaluation and assignment of free carrier density is difficult. Recently, Nan et al. [12] used the IR reflectance technique for the qualitative determination of free carrier density in ZnO films.

In ZnO, there exists an absorption in between its electronic absorption band (around 0.40 μm) and deep lattice absorption band (around 25 μm) which is sensitive to the free carrier density and for which the IR reflectivity approaches zero. The intensity and the characteristic frequency of this band in the absorption spectra depend strongly on the free carrier density.

In this work we present an IR absorption study of the free carriers in ZnO nanocomposite films produced by incorporation of several metal and semiconductor nanoclusters in ZnO matrix. The nanocomposite films are prepared either by co-sputtering or by alternate sputtering of metals or semiconductors and ZnO targets with different metal/semiconductor contents and then annealed at different temperatures. X-ray diffraction (XRD) and transmission electron microscopy (TEM) techniques are used to study the crystalline quality and morphology of the nanocomposites.

2. Experimental

Composite films of metal/semiconductor–ZnO are prepared on well cleaned quartz substrates by co-sputtering of metal/semiconductor co-targets and a ZnO target (50 mm

* Corresponding author. Fax: +52 222 2295611.
E-mail address: upal@sirio.ifaup.buap.mx (U. Pal).

0040-6090/$ - see front matter © 2005 Published by Elsevier B.V.
doi:10.1016/j.tsf.2005.04.045

diameter, 99.999% purity) at fixed argon (Ar) gas pressure and 100 W r.f. power. For the metal–ZnO composites, Au and Pt wires of 0.4 mm diameter and of different lengths are placed on the ZnO target and co-sputtered for 2 hrs at 4 mTorr Ar pressure. For the Si–ZnO composite films, Si co-targets ($5\times5\times0.3$ mm wafers) of different numbers are placed on the main ZnO target symmetrically and co-sputtered at 10 mTorr Ar pressure for 1 hr. Ge–ZnO nanocomposites are prepared by alternate sputtering of ZnO and Ge targets at 45 mTorr argon pressure for 82 min. The details of the sample preparation technique are reported in our earlier works [13–16]. The composite films are annealed in a tubular furnace at different temperatures in argon atmosphere for 2 h. For TEM study, the samples are prepared on carbon coated Cu micro grids for shorter time of deposition and annealed at different temperatures as mentioned earlier. A JEOL-2010 (or JEOL JEM2000-FXII) electron microscope was used for the TEM observations on the samples. XRD patterns were recorded using Cu-K_α radiation of a Rigaku RAD-C (or Bruker) diffractometer. A Nicolet Magna 750 FTIR spectrometer was used to record the IR spectra.

3. Results and discussion

From the TEM micrographs we can observe the formation of homogeneously distributed nanoparticles in the ZnO matrix. In general, for the Si/ZnO and Au/ZnO composite films the average size of the nanoparticles increased with the increase of annealing temperature (Figs. 1 and 2). Whereas, the increase of Si or Au content in the composite films caused only an increase in the density of the particles, without causing any significant change in their average size [13,14]. Fig. 3 shows the typical TEM micrographs of the as-deposited Pt/ZnO films prepared with 3 pieces of Pt wires of 15 mm length and after annealing at 200 °C and 600 °C. In the as-deposited films we can observe the agglomeration of small particles to form very

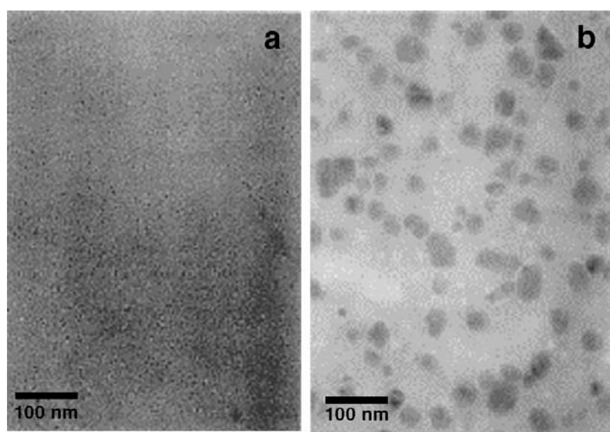

Fig. 1. Typical TEM micrographs of Si/ZnO composites prepared with 12 pieces of Si and annealed at a) 400 °C and b) 800 °C.

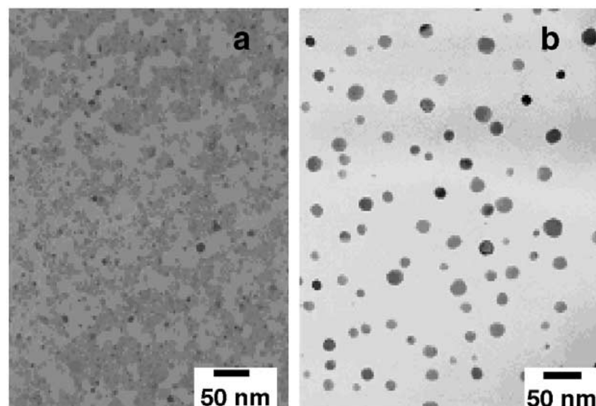

Fig. 2. TEM micrographs of Au/ZnO composites prepared with 3 pieces of Au wires of 7.5 mm length and annealed at a) 500 °C and b) 700 °C.

big clusters with average size of 275 nm. On annealing at 200 °C or higher temperatures, a homogeneous distribution of small Pt particles in the ZnO matrix is observed due to the disintegration of the big clusters (in as-grown samples). On annealing at 600 °C, the small particles aggregated to form particles with an average size of 6.4 nm. But, for the Ge/ZnO composite films, with the increase of annealing temperature the average size of the Ge particles decreased. The average size varied from 5 nm for as-deposited films to 2.3 nm for films annealed at 600 °C [15].

In Fig. 4a, the evolution of the XRD spectrum with the variation of Au content for Au/ZnO composites films annealed at 700 °C is shown. With increase of Au content, the intensity of the peaks related to the (111) and (220) planes of Au increased. There appeared a peak corresponding to the formation of Au_2O_3, intensity of which decreased with the increase of Au content in the films. Fig 4b shows the XRD patterns for the Au/ZnO composite films before and after annealing at different temperatures. With the increase of annealing temperature, the intensity of the (002) and (103) reflections of ZnO increased. However, the intensity of the reflection corresponds to oxidized Au (AuO and Au_2O_3) decrease and the intensity of the (111) reflection corresponds to Au increased. It is clear that on increasing the annealing temperature, the Au in oxidized state is reduced to metallic gold.

Fig. 5 shows the XRD patterns for the Si/ZnO composite films. With the increase of Si content, the crystallinity of the composite films decreases. On the other hand, with the increase of annealing temperature, the crystallinity of the films increases. Infrared measurements revealed the bands correspond to the modes of vibration of the metal (or semiconductor) nanoparticles and ZnO. The evolution of the IR bands (shape, intensity and shift) of the semiconductor nanoparticles with the variation of the growth parameters has been reported in several articles [13,17,18]. Fig. 6 shows the IR reflectance spectra in the spectral range of 550–900 cm^{-1} for the X/ZnO nanocomposites. In general, the spectra reveal a broad band

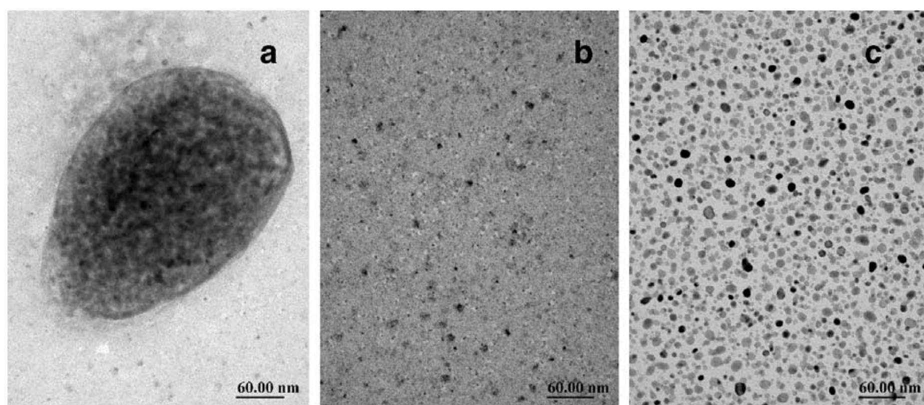

Fig. 3. Typical TEM micrographs of Pt/ZnO nanocomposite films prepared with 3 pieces of Pt of 15 mm length: a) as-deposited, b) annealed at 200 °C and c) annealed at 600 °C.

between 589 and 645 cm^{-1}, which is sensitive to the presence of free charge carriers in the films. The characteristic frequency of this band is affected by the content and kind of materials incorporated in the ZnO matrix and the density of free carriers generated. IR spectra of the Ge/ZnO composites films revealed that the position of the band shifts from 589 cm^{-1} for as-deposited films to 598 cm^{-1} for the films annealed at 600 °C, whereas, the reflectance increased on annealing (Fig. 6a). The shift towards higher frequencies is due to increase in free carrier density on annealing. With the increase of the annealing temperature, some of the Ge nanoparticles oxidize, leaving oxygen vacancies in the ZnO matrix causing an increase in the free carrier concentration. Generally, the increase in the free carriers causes a decrease in the reflectance due to higher free carrier absorption. However, the observed increase of reflectance on Ge/ZnO composites on annealing might be due to its high porosity [12].

In comparison with Ge/ZnO composites, the reflection band in Si/ZnO composites has lower reflectivity and its position shifts from 635 cm^{-1} to 656 cm^{-1} on annealing the films at 800 °C (Fig. 6b). The reason may be that Si/ZnO films have higher free carrier concentration as the Si incorporated in the ZnO almost completely remained in the SiO_X ($0<X<2$) chemical state [13,19].

In Au/ZnO films the reflectance band is localized at higher frequencies, which is attributed to increase of free carrier density in ZnO due to the metal incorporation. There appeared no sharp reflectance minima in this frequency interval for the Pt/ZnO composite films. The IR spectra of Au/ZnO composite films reveal that the band localized around 650 cm^{-1} in as-deposited films shifts towards lower frequencies (640 cm^{-1}) on annealing the films at 800 °C with an increase in its intensity. In case of Pt/ZnO composites, there were no noticeable changes in the reflectance spectra on annealing.

On annealing the Au/ZnO composites, due to the reduction of oxide states of Au, the density of free charge carriers in ZnO decreases; causing a shift in frequency of absorption band (Fig. 6d) towards lower values. In case

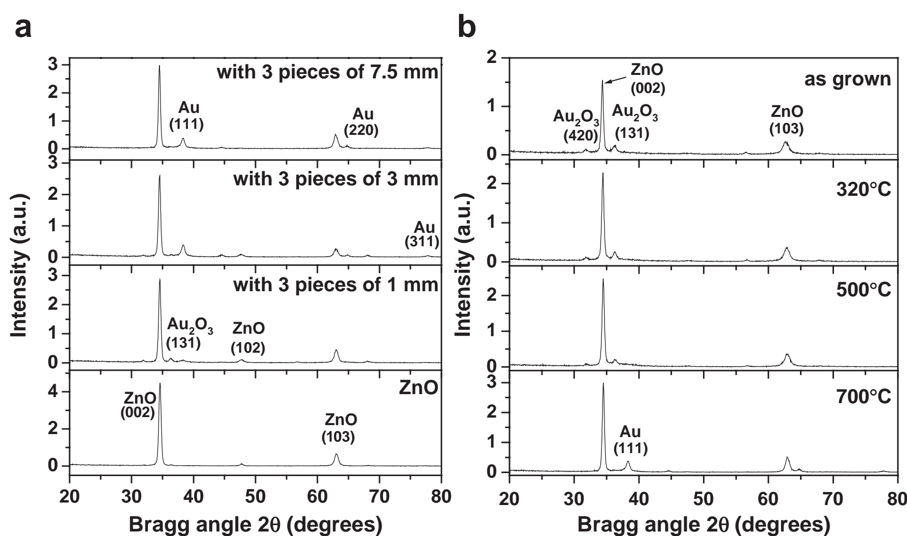

Fig. 4. XRD patterns of the Au/ZnO nanocomposites: a) prepared with different Au content and treated at 700 °C, b) prepared with 3 pieces of Au wires of 7.5 mm and annealed at different temperatures.

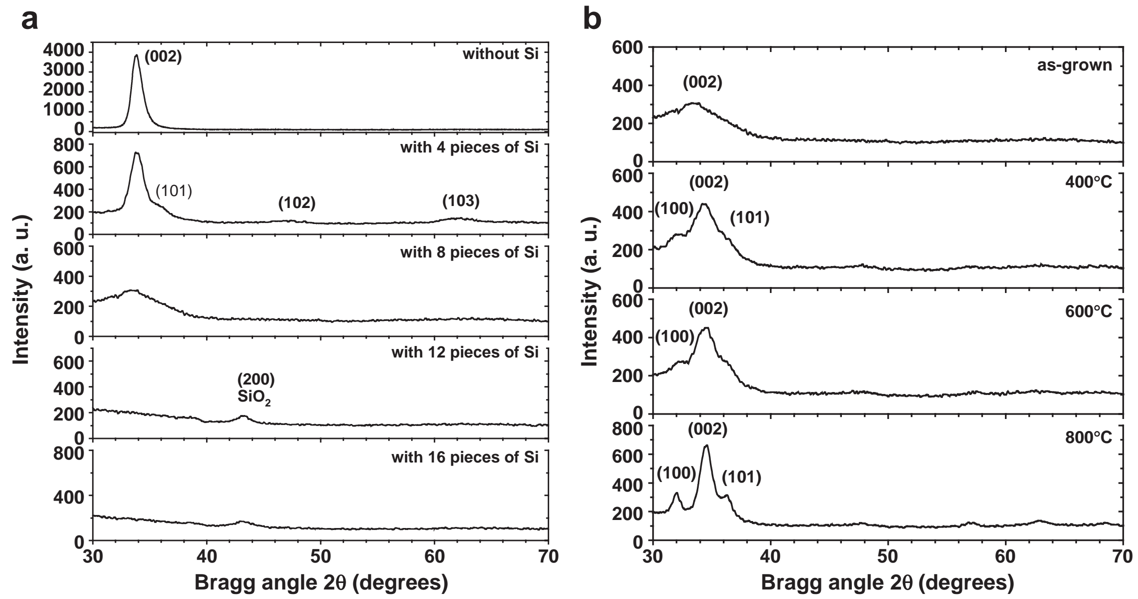

Fig. 5. XRD patterns of the Si/ZnO nanocomposites: a) prepared with different Si content and b) prepared with 8 pieces of Si and annealed at different temperatures. All the identified planes except SiO_2 are related to ZnO matrix.

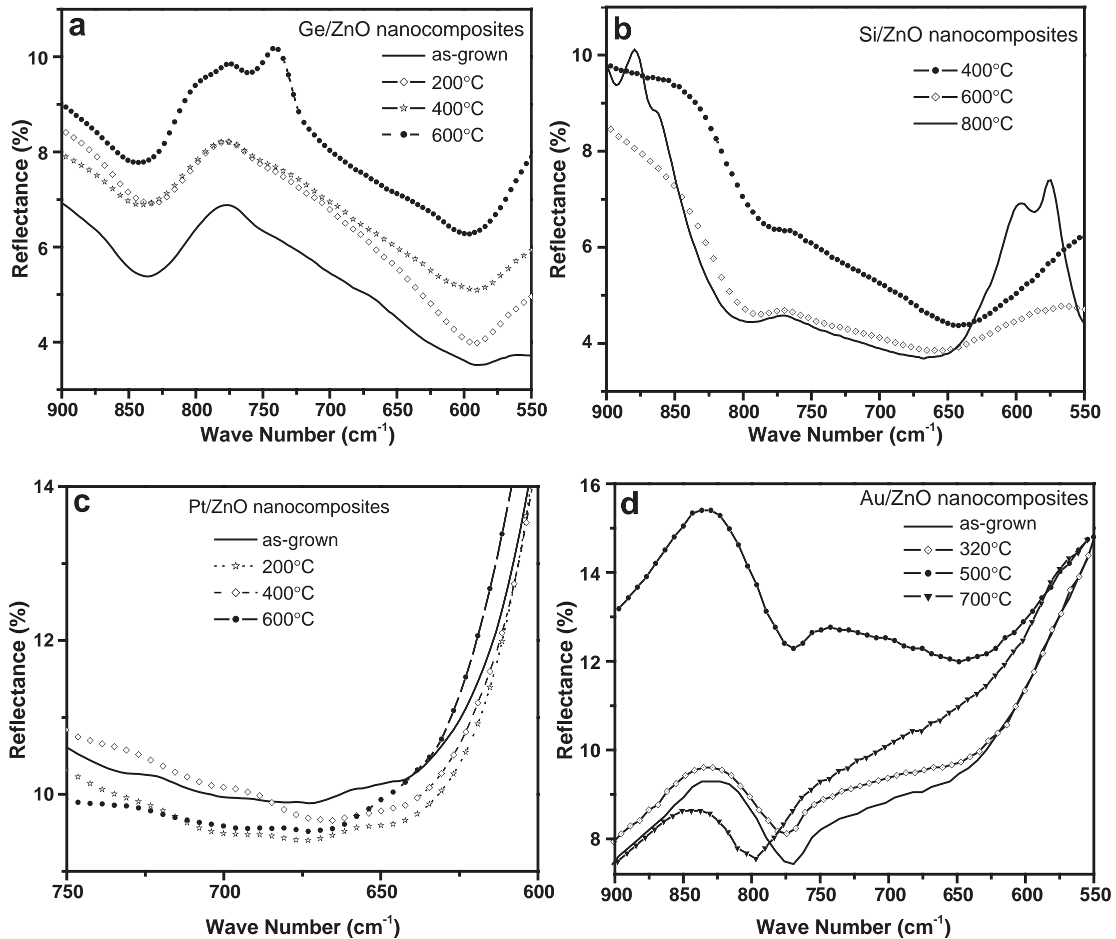

Fig. 6. IR spectra of the nanocomposite films annealed at different temperatures: a) Ge/ZnO, b) Si/ZnO, c) Pt/ZnO and d) Au/ZnO.

of Pt/ZnO, as Pt remains in the composites without forming any oxide, there is no significant change in the free carrier concentration of ZnO matrix on annealing (Fig. 6c).

4. Conclusions

X (Au, Pt, Si or Ge)/ZnO nanocomposite films were prepared by r.f. co-sputtering. IR spectra of the X/ZnO composites revealed an absorption band which is sensitive to the presence of free charge carriers in the films. The position and intensity of the IR band depend on the material incorporated in the matrix and the annealing temperature. For the metals or semiconductors which get oxidized upon incorporating them in ZnO matrix, the free carrier concentration in ZnO increases causing a shift of the IR band towards higher frequencies. While for the non-oxidizing elements, the IR absorption band has no effect on the incorporation of metal or semiconductor guests. Therefore, just by monitoring a single reflectance band in the IR spectra of ZnO, it is possible to monitor the oxidation state of the incorporated species.

Acknowledgement

The work is partially supported by VIEP-SEP-CONACyT, Mexico (Grant No. II 194-04/EXC/I).

References

[1] T. Minami, H. Nanto, S. Takata, Thin Solid Films 124 (1985) 43.
[2] L. Bahadur, M. Hamdani, J.F. Koenig, P. Chartier, Sol. Energy Mater. 14 (1985) 107.
[3] Z.-C. Jin, I. Hamberg, C.G. Granqvist, B.E. Sernelius, K.-F. Berggrem, Thin Solid Films 164 (1988) 381.
[4] S. Pizzini, N. Butta, D. Narducci, M. Palladito, J. Electrochem. Soc. 136 (1989) 1945.
[5] N. Yamazoe, Sens. Actuators, B, Chem. 5 (1991) 7.
[6] G.S. Kino, R.S. Wagers, J. Appl. Phys. 44 (1973) 1480.
[7] D.C. Look, Mater. Sci. Eng., B, Solid-State Mater. Adv. Technol. 80 (2001) 383.
[8] R. Ondo.Ndong, F. Pascal-Delannoy, A. Boyer, A. Giani, A. Foucaran, Mater. Sci. Eng., B, Solid-State Mater. Adv. Technol. 97 (2003) 68.
[9] S.B. Majumder, M. Jain, P.S. Dobal, R.S. Katiyar, Mater. Sci. Eng., B, Solid-State Mater. Adv. Technol. 103 (2003) 16.
[10] B.P. Zhang, N.T. Binh, K. Wakatsuki, Y. Segawa, Y. Kashiwaba, K. Haga, Nanotechnology 15 (2004) S382.
[11] X.Y. Kong, Y. Ding, R. Yang, Z.L. Wang, Science 303 (2004) 1348.
[12] C.-W. Nan, R. Birringer, W. Krauss, H. Gao, H. Gleiter, Phys. Status Solidi 162 (1997) R3.
[13] U. Pal, J. García-Serrano, Solid State Commun. 111 (1999) 427.
[14] U. Pal, E. Aguila-Almanza, O. Vázquez-Cuchillo, N. Koshizaki, T. Sasaki, S. Terauchi, Sol. Energy Mater. Sol. Cells 70 (2001) 363.
[15] U. Pal, G. Casarrubias-Segura, O. Zarate-Corona, Sol. Energy Mater. Sol. Cells 76 (2003) 305.
[16] U. Pal, J. García-Serrano, G. Casarrubias-Segura, N. Koshizaki, T. Sasaki, S. Terauchi, Sol. Energy Mater. Sol. Cells 81 (2004) 339.
[17] J. García-Serrano, U. Pal, N. Koshizaki, T. Sasaki, Rev. Mex. Fis. 47 (2001) 26.
[18] U. Pal, J. García-Serrano, Appl. Surf. Sci. (2005) (published online).
[19] U. Pal, N. Koshizaki, S. Terauchi, T. Sasaki, Microsc. Microanal. Microstruct. 8 (1997) 403.